Visualization of the variability of 3D statistical shape models by animation

Hans Lamecker, Martin Seebaß, Thomas Lange, Hans-Christian Hege, Peter Deuflhard
Zuse–Institute–Berlin (ZIB),
Takustr. 7, 14195 Berlin, Germany

Abstract. Models of the 3D shape of anatomical objects and the knowledge about their statistical variability are of great benefit in many computer assisted medical applications like images analysis, therapy or surgery planning. Statistical model of shapes have successfully been applied to automate the task of image segmentation. The generation of 3D statistical shape models requires the identification of corresponding points on two shapes. This remains a difficult problem, especially for shapes of complicated topology. In order to interpret and validate variations encoded in a statistical shape model, visual inspection is of great importance. This work describes the generation and interpretation of statistical shape models of the liver and the pelvic bone.

1 Introduction

Models of the 3D shape of anatomical objects and the knowledge about their statistical variability are of great benefit in many computer assisted medical applications like images analysis, therapy or surgery planning. Statistical model of shapes have successfully been applied to automate the task of image segmentation, see for instance [1] and references therein. They consist of a mean shape plus the main modes of deviations from this mean.

The generation of 3D statistical shape models requires the identification of corresponding points on two shapes, which is often referred to as the *correspondence problem*. This remains a difficult problem, especially for shapes of complicated topology. In this work we describe the process of generating shape models from objects of arbitrary topology [1] and present two examples: a statistical model of the liver and the pelvic bone shape.

In order to interpret and validate variations encoded in a statistical shape model, visual inspection is of great importance. We propose to animate the shape modes of the statistical models to get a visual impression of the deviations away from the mean shape. Note that there are means to assess the quality of a statistical shape model that should always precede visual inspection, such as the compactness and the completeness of a model. This however is not the subject of this work. Please refer to [2] instead.

This paper is organized as follows: section 2 provides the theory of statistical shape modeling. The method of establishing corresponding points on different shapes is described in section 3. Section 4 presents two examples of statistical shape models and their analysis. Finally we conclude in section 5.

2 Statistical Shape Models

A statistical model is built from a training set of shapes $\boldsymbol{v}_i$ ($i = 1, \ldots, N$). Each shape $\boldsymbol{v}_i$ is given by M points sampled on its surface (thus $\boldsymbol{v}_i \in \mathbb{R}^{3M}$). Using principal component analysis each shape vector can be expressed using a linear model of the form

$$\boldsymbol{v}_i = \overline{\boldsymbol{v}} + \boldsymbol{P}\boldsymbol{b}_i = \overline{\boldsymbol{v}} + \sum_k \boldsymbol{p}^k b_i^k \tag{1}$$

where $\overline{\boldsymbol{v}}$ is the mean shape vector and $\boldsymbol{P} = \{\boldsymbol{p}^k\}$ the matrix of eigenvectors of the covariance matrix. The corresponding eigenvalues $\{\lambda^k\}$ describe the amount of variance in the direction of the eigenvectors. The shape parameters $\boldsymbol{b} = \{b^k\}$ control the modes of variation.

In order to obtain a correct statistical model all M points on each surface (a) must correspond in an anatomical meaningful way, *and* (b) their coordinates must be given relative to a common frame of reference (alignment). This is crucial, since incorrect correspondences can either introduce too much variation or lead to illegal instances of the model.

Note that - in general - these two goals can be accomplished independently of one another. Often, however, an initial alignment precedes the computation of corresponding points (e.g. when corresponding points are supposed to be closest points). In this work we will employ a method, that does *not* rely on an initial alignment (see section 3). Once correspondence has been established, the alignment will be computed in the following way:

Without loss of generality, let $\boldsymbol{v}_1$ define the reference coordinate system, which all other shapes $\boldsymbol{v}'_j$ ($j > 1$) will be aligned to. Let $\boldsymbol{x}_{1,k}$ denote the coordinates of the shape vector $\boldsymbol{v}_1$, and $\boldsymbol{x}'_{j,k}$ the coordinates of $\boldsymbol{v}'_j$ respectively. Then we compute a rigid transformation $\boldsymbol{T}_{j,\min}$ that minimizes the sum of squared distances between corresponding pairs $\boldsymbol{x}_{1,k}$ and $\boldsymbol{x}'_{j,k}$ ($k = 1, \ldots, M$), for all $j > 1$:

$$\boldsymbol{T}_{j,\min} = \arg\min_{\boldsymbol{T}} \sum_{k=1}^{M} \|\boldsymbol{x}_{1,k} - \boldsymbol{T}\boldsymbol{x}'_{j,k}\|^2$$

This minimization problem can be solved by singular value decomposition [3]. The coordinates of the final shape vector $\boldsymbol{v}_j$ will then be $\boldsymbol{x}_{j,k} = \boldsymbol{T}_{j,\min}\boldsymbol{x}'_{j,k}$.
This procedure introduces some bias towards the reference system $\boldsymbol{v}_1$, which can be reduced by iterative refinement (see e.g. [4]). However we have seen in our experiments that the influence of this defect is rather small.

3 Solving the correspondence problem

The task of establishing correspondence between two topologically equivalent 3D shapes $\mathcal{S}_1, \mathcal{S}_2$, represented as triangular meshes, is to compute a homeomorphic mapping

$$f : \mathcal{S}_1 \rightarrow \mathcal{S}_2 ,$$

possibly under additional constraints (e.g. specifically given correspondences of points or lines of anatomical or geometrical significance). Depending on these constraints, there may

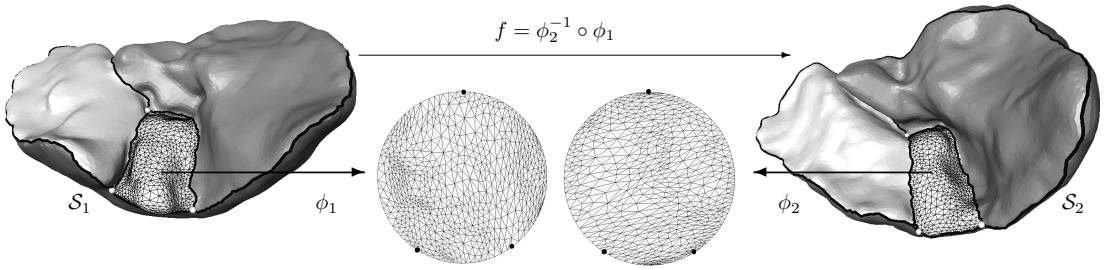

Figure 1: A homeomorphism f between the shapes $\mathcal{S}_1$ and $\mathcal{S}_2$ is computed by mapping each patch of the two shapes onto a disc using the shape preserving mappings ϕ_1 and ϕ_2 respectively. The boundaries are mapped to the unit circle by fixing all branch points according to their average arc-length on both surfaces to be matched. All edges on the boundaries are mapped according to their arc-length on the original surfaces. The resulting mapping for one patch is given by $f = \phi_2^{-1} \circ \phi_1$.

be many solutions to this problem. Hence there is a need to impose further restrictions, that define optimal correspondences.

Since we are dealing with anatomical shapes, we propose that f is required to introduce as little distortion as possible, i.e. preserve the metric structure of $\mathcal{S}_1$ by approximately keeping angles fixed and allowing for global scaling of $\mathcal{S}_1$.

Instead of computing f directly we define a canonical base domain D to which each of the shapes $\mathcal{S}_1$ and $\mathcal{S}_2$ is mapped. D must be homeomorphic to $\mathcal{S}_1$ or $\mathcal{S}_2$.

$$\begin{array}{ccc} \mathcal{S}_1 & \xrightarrow{f_2^{-1} \circ f_1} & \mathcal{S}_2 \\ & {\scriptstyle f_1} \searrow \quad \swarrow {\scriptstyle f_2} & \\ & D & \end{array} \tag{2}$$

Hence we are left with the problem of finding a mapping $f : \mathcal{S}_i \rightarrow D$ for each shape i, consistent with the constraints given.

Surfaces homeomorphic to discs. Let us consider the easiest case, where $\mathcal{S}_1$ and D are homeomorphic to a disc. Moreover let $D \subset \mathbb{R}^2$ be a convex region. As an additional constraint, we require the boundary of $\mathcal{S}_1$ to be mapped smoothly to the boundary of D.

We use *convex-combination maps* [5] to flatten $\mathcal{S}_1$ to D. Without loss of generality, let $X = \{\boldsymbol{x}_1, \ldots, \boldsymbol{x}_n, \boldsymbol{x}_{n+1}, \ldots, \boldsymbol{x}_N\}$ be the coordinates of the vertices of the surface triangulation $\mathcal{S}_1$. Assume that $\boldsymbol{x}_1, \ldots, \boldsymbol{x}_n$ are internal nodes, while $\boldsymbol{x}_{n+1}, \ldots, \boldsymbol{x}_N$ lie on the boundary. Furthermore let $\boldsymbol{u}_i \in D \subset \mathbb{R}^2$ ($i = 1, .., N$) be the corresponding coordinates in the parameter domain. The mapping

$$\phi : X \rightarrow D, \ \boldsymbol{x}_i \mapsto \boldsymbol{u}_i = \phi(\boldsymbol{x}_i)$$

is called a *convex combination map*, if

$$\boldsymbol{u}_i = \sum_{j=1}^{N} \lambda_{ij} \boldsymbol{u}_j \tag{3}$$

for all internal nodes $i = 1, \ldots, n$, and

$$\sum_{j=1}^{N} \lambda_{ij} = 1 \quad , \quad \lambda_{ij} \begin{cases} = & 0 & (i,j) \notin E \\ > & 0 & (i,j) \in E \end{cases} \tag{4}$$

where E is the set of all edges of the triangulation. It was shown by Floater [5] that ϕ does not produce any fold-overs in the planar triangulation, and every node $\boldsymbol{u}_i$ lies in the convex hull of ∂D. Computing ϕ amounts to solving the linear system (3) under the constraints of (4). Floater also showed that there exists a unique solution to this problem. Since (3) is a sparse linear system of equations, it can be solved efficiently.

The question remains on how to choose the convex combination weights λ_{ij}. We are interested in producing a mapping, that preserves the metric structure of the surface $\mathcal{S}_1$ as good as possible. We use here the idea of locally approximating the *geodesic polar map* [6], first presented by Floater [5]. Thereby λ_{ij} are computed as convex weights in the planar domain, such that the angles and lengths of the original triangulation are preserved as good as possible The resulting map is called *shape preserving map*. Please refer to [5] for details.

Arbitrary surfaces. To establish correspondence between two arbitrary surfaces, we employ a method presented by Zöckler et al. [7]. An arbitrary surface is thereby divided into patches, each homeomorphic to a disc. This decomposition needs not only to be topologically equivalent on all surfaces of the training set but also to represent similar anatomical regions in order to get a meaningful correspondence. Each corresponding pair of patches is mapped onto a common planar convex base domain. We choose the unit disc (radius 1, centered at the origin). To achieve continuity across patch borders the patch boundaries are mapped to the unit circle according to their average arc-length on the two surfaces to be matched (see figure 1). Branch points (vertices, that belong to more than one boundary) are thus fixed on the circle, while all boundary edges are mapped according to the arc-length on their original surface. If we repeat the procedure for each pair of patches, we obtain a mapping from each vertex of $\mathcal{S}_1$ onto the surface of $\mathcal{S}_2$.

The patch decomposition is an interactive process. The patch boundaries are drawn on the surface by manually selecting points where two or more patch boundaries would meet (branch points). Some intermediate points along the patch boundaries may be added manually. These points are then automatically connected by computing geodesic shortest paths between them. In almost all cases we use a metric that favors paths along lines of high curvature, when these lines represent anatomical features. In other cases we use a pure distance measure. Note that since the definition of the patch boundaries is independent of the location and orientation of the surface in space, the whole process of establishing correspondences does not rely on any initial alignment of the surfaces.

4 Results

We have generated two statistical shape models using the procedure described above: one of the *liver* from 43 shapes of male and female patients (based on preliminary work presented in [2]) and another one of the *pelvic bone* from 23 CT data sets of male patients.

The liver surface was divided into four patches (figure 2 left):

- the lower border of the left lobe (LL),
- the lower border of the right plus the caudate lobe (LR+CL),

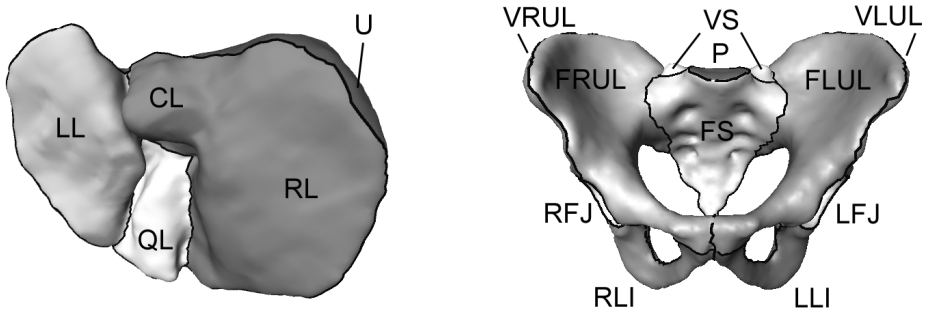

Figure 2: Liver and pelvic bone decomposition.

- the lower border of the quadratic lobe (QL) and
- the whole upper part of the liver surface (U)

Following the procedure described in section 3 the user had to specify no more than 10 landmarks per surface, resulting in 4 patches, divided by 6 patch boundaries and 4 branch points.

The pelvic bone surface was divided into 11 patches (figure 2 right):

- the promontorium (P)
- the frontal/ventral sacrum (FS, VS)
- the frontal right/left upper ilium (FRUL, FLUL)
- the ventral right/left upper ilium (VRUL, VLUL)
- the right/left femur joint (RFJ, LFJ)
- the right/left lower ilium (RLI, LLI)

The manual interaction is more demanding in this case, due to the complicated topology of the object (genus=3). The user had to specify about 40 landmarks per surface, resulting in 11 patches, divided by 40 patch boundaries and 25 branch points.

The compactness and completeness of these models has been tested elsewhere [2, 8]. The results show that these models are not complete yet, however increasing the training set has lead to steady improvements.

In order to visualize the variability of a statistical model we propose to animate the model in two ways: (a) by deforming the mean shape continuously into the training shapes and (b) by varying the main modes of variation continuously.

The main modes of variation of the liver model (figure 3) can be interpreted as: (1) change of volume, (2) change of relative size between left and right lobe and (3) scaling in z-direction. The main mode of variation of the pelvic bone (figure 4) model can be described as: (1) scaling in z-direction, (2) widening and bending of the ilium and (3) change of length of the sacrum. Movie files of the animations can be downloaded from [9].

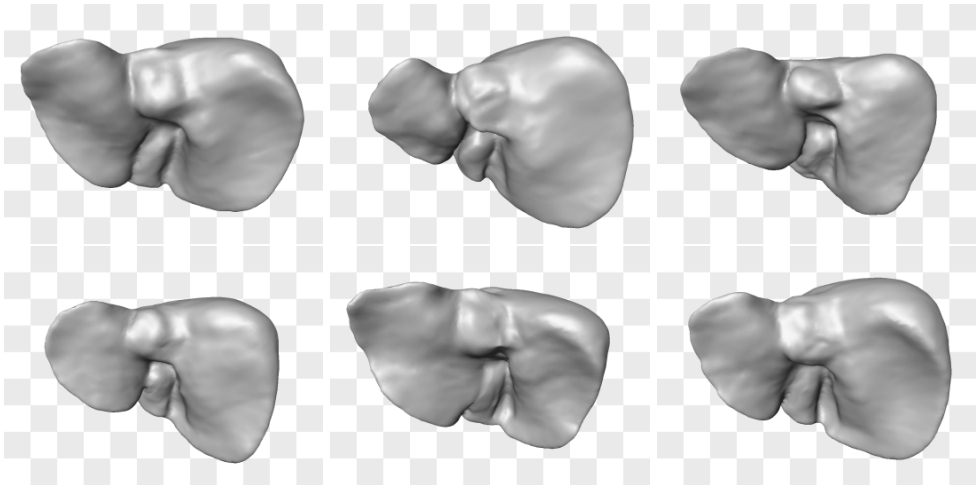

Figure 3: Variability of a statistical model of the liver shape made from 43 training data sets: in the left column the eigenmode with the largest variance λ_1 is varied between $\pm 3\sqrt{\lambda_1}$, in the second and third column the modes with the second and third largest variance are shown respectively.

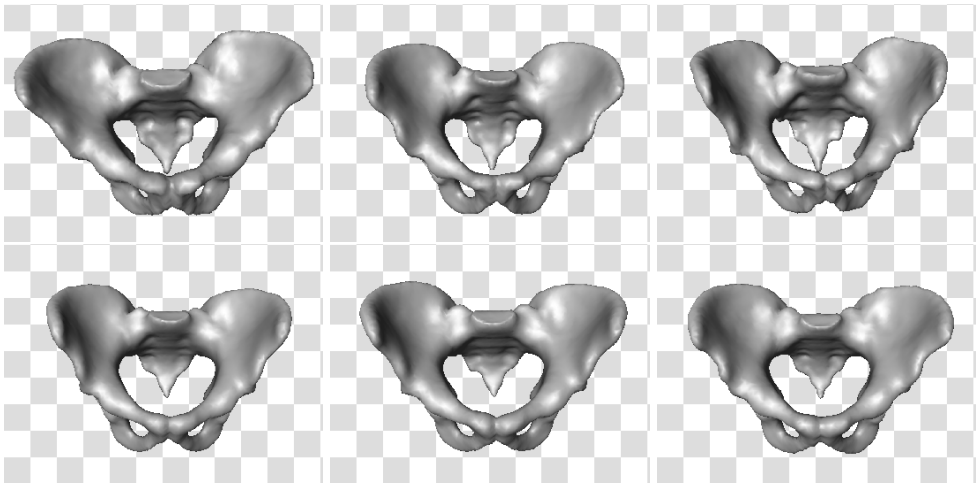

Figure 4: Variability of a statistical model of the pelvic bone shape made from 23 training data sets: in the left column the eigenmode with the largest variance λ_1 is varied between $\pm 3\sqrt{\lambda_1}$, in the second and third column the modes with the second and third largest variance are shown respectively.

5 Conclusions and Discussion

We have shown how to construct statistical shape models of objects of arbitrary topology. Although the process is not fully automatic, manual interaction allows experts to incorporate their knowledge about matching regions on two shapes.

The visualization of statistical shape models of the liver and the pelvic bone reveal modes of variation that can be interpreted quite well in anatomical terms. Due to the large variability of the liver shape this was not be expected - in contrast to the pelvic bone, which is a rigid object. This indicates that the correspondence method used here works well.

Animating statistical shape models allows for an intuitive visual inspection of anatomical shape changes. We demonstrated this for two statistical models of the liver and pelvic bone respectively. In the future we want to

- extend these models by enlarging the training set,
- compare different correspondence methods and
- use different statistical methods to extract the main modes of variation.

and investigate how this parameters change the interpretation of the modes of variation of the statistical shape models.

Acknowledgements

This work was supported by the DFG Research Center ”Mathematics for key technologies” (FZT 86) in Berlin.

References

[1] Hans Lamecker, Thomas Lange, and Martin Seebaß. A statistical shape model for the liver. In *MICCAI 2002*, pages 422–427, 2002.

[2] Hans Lamecker, Thomas Lange, Martin Seebaß, Sebastian Eulenstein, Malte Westerhoff, and Hans-Christian Hege. Automatic segmentation of the liver for the preoperative planning of resections. In *MMVR 2003*, volume 94, pages 171–174, 2003.

[3] A. D. McLachlan. Least squares fitting of two structures. *J. Mol. Biol.*, 128:74–79, 1979.

[4] Alejandro F. Frangi, Daniel Rückert, Julia A. Schnabel, and Wiro J. Niessen. Construction of multiple-object three-dimensional statistical shape models: Application to cardiac modelling. *IEEE Transactions on Medical Imaging*, 21(9):1151–1166, 2002.

[5] Michael S. Floater. Parameterization and smooth approximation of surface triangulations. *Computer Aided Geometric Design*, 14(3):231–250, 1997.

[6] Barrett O’NEILL. *Elementary differential geometry*. Academic press, 1966.

[7] Malte Zöckler, Detlev Stalling, and Hans-Christian Hege. Fast and intuitive generation of geometric shape transitions. *The Visual Computer*, 16(5):241–253, 2000.

[8] Martin Seebaß, Hans Lamecker, Thomas Lange, Johanna Gellermann, and Peter Wust. A statistical shape model for segmentation of the pelvic bone. In *ESHO 2003 - 21th Annual Meeting of the European Society of Hyperthermic Oncology*, pages 91–93, 2003.

[9] Hans Lamecker. Model based image segmentation. URL: http://www.zib.de/visual/projects/index.html, October 2003.